

Article

Dosimetry of a Novel ¹¹¹Indium-Labeled Anti-P-Cadherin Monoclonal Antibody (FF-21101) in Non-Human Primates

Gregory Ravizzini ^{1,*}, William Erwin ², Louis De Palatis ^{3,†}, Lucia Martiniova ⁴, Vivek Subbiah ^{5,‡}, Vincenzo Paolillo ⁶, Jennifer Mitchell ⁷, Asa P. McCoy ¹, Jose Gonzalez ¹ and Osama Mawlawi ²

- ¹ Department of Nuclear Medicine, University of Texas MD Anderson Cancer Center, 1400 Pressler St., Unit 1483, Houston, TX 77030, USA; jagonzalez1@mdanderson.org (J.G.)
- ² Department of Imaging Physics, Division of Diagnostic Imaging, University of Texas MD Anderson Cancer Center, Houston, TX 77030, USA; werwin@mdanderson.org (W.E.); omawlawi@mdanderson.org (O.M.)
- ³ Technology and Business Development, Center for Advanced Biomedical Imaging, University of Texas MD Anderson Cancer Center, Houston, TX 77030, USA; ldp.biodev@gmail.com
- ⁴ Department of Experimental Therapeutics, University of Texas MD Anderson Cancer Center, Houston, TX 77030, USA; lmartini@mdanderson.org
- ⁵ Department of Investigational Cancer Therapeutics, Division of Cancer Medicine, University of Texas MD Anderson Cancer Center, Houston, TX 77030, USA
- ⁶ Cyclotron Radiochemistry Facility, Center for Advanced Biomedical Imaging, University of Texas MD Anderson Cancer Center, Houston, TX 77030, USA; vincenzo.paolillo@mdanderson.org
- ⁷ Department of Veterinary Medicine and Surgery, University of Texas MD Anderson Cancer Center, Houston, TX 77030, USA; jmitchell2@mdanderson.org
- * Correspondence: gravizzini@mdanderson.org; Tel.: +1-713-745-5721
- † Current address: BioDevelopment Solutions, LLC, Johnstown, CO 80534, USA.
- ‡ Current address: Sarah Cannon Research Institute, Nashville, TN 37203, USA.



Citation: Ravizzini, G.; Erwin, W.; De Palatis, L.; Martiniova, L.; Subbiah, V.; Paolillo, V.; Mitchell, J.; McCoy, A.P.; Gonzalez, J.; Mawlawi, O. Dosimetry of a Novel ¹¹¹Indium-Labeled Anti-P-Cadherin Monoclonal Antibody (FF-21101) in Non-Human Primates. *Cancers* **2023**, *15*, 4532. <https://doi.org/10.3390/cancers15184532>

Academic Editor: Michael L. F. Lerch

Received: 11 July 2023

Revised: 27 August 2023

Accepted: 5 September 2023

Published: 13 September 2023



Copyright: © 2023 by the authors. Licensee MDPI, Basel, Switzerland. This article is an open access article distributed under the terms and conditions of the Creative Commons Attribution (CC BY) license (<https://creativecommons.org/licenses/by/4.0/>).

Simple Summary: This research study focuses on the P-cadherin protein, which is found in many types of tumors, and could be a potential target for therapy. FF-21101, a human–mouse chimeric monoclonal antibody that targets P-cadherin, was labeled with indium-111 (¹¹¹In) and investigated for biodistribution and radiation doses in six cynomolgus macaques. To assess the radiation profile distribution and clearance of FF-21101 (¹¹¹In), we performed whole-body imaging and generated time–activity curves. The lungs, spleen, liver, kidneys, and heart wall received the highest radiation dose estimates for FF-21101 (¹¹¹In). These findings led us to estimate the radiation doses that would be delivered to different organs if this antibody was labeled with yttrium-90 (⁹⁰Y) and used in targeted radioimmunotherapy in patients. FF-21101 shows potential for clinical application in humans, according to biodistribution data obtained from macaques. Based on these results, an investigational new drug application was filed with the FDA for a Phase I clinical trial.

Abstract: P-cadherin is associated with a wide range of tumor types, making it an attractive therapeutic target. FF-21101 is a human–mouse chimeric monoclonal antibody (mAb) directed against human P-cadherin, which has been radioconjugated with indium-111 (¹¹¹In) utilizing a DOTA chelator. We investigated the biodistribution of FF-21101 (¹¹¹In) in cynomolgus macaques and extrapolated the results to estimate internal radiation doses of ¹¹¹In- and yttrium-90 (⁹⁰Y)-FF-21101 for targeted radioimmunotherapy in humans. Whole-body planar and SPECT imaging were performed at 0, 2, 24, 48, 72, 96, and 120 h post-injection, using a dual-head gamma camera. Volumes of interest of identifiable source organs of radioactivity were defined on aligned reference CT and serial SPECT images. Organs with the highest estimated dose values (mSv/MBq) for FF-21101 (¹¹¹In) were the lungs (0.840), spleen (0.816), liver (0.751), kidneys (0.629), and heart wall (0.451); and for FF-21101 (⁹⁰Y) dose values were: lungs (10.49), spleen (8.21), kidneys (5.92), liver (5.46), and heart wall (2.61). FF-21101 (¹¹¹In) exhibits favorable biodistribution in cynomolgus macaques and estimated human dosimetric characteristics. Data obtained in this study were used to support the filing of an investigational new drug application with the FDA for a Phase I clinical trial.

Keywords: *CDH3*; SPECT; non-human primates; radioimmunotherapy; internal radiation dosimetry; theranostics

1. Introduction

Cadherins are cell–cell adhesion glycoproteins that form calcium-dependent intercellular junctions and play an essential role in morphogenesis, development, and maintenance of the integrity of tissues and organs [1]. The cadherin family is subdivided into various subfamilies, including the classical E-, P-, and N-cadherins, each demonstrating a specific tissue distribution [2]. E-cadherin is expressed in all epithelial tissues; however, the expression of P-cadherin is restricted to the basal or inner layers of stratified epithelia, including prostate and skin, and to breast myoepithelial cells [3]. Several studies have demonstrated that aberrant P-cadherin expression is associated with cell proliferation and with tumors of the colon, breast, lung, thyroid, pancreas, and cervix, making P-cadherin (encoded by the gene *CDH3*) an excellent tumor-associated target [4,5].

The development of P-cadherin anticancer therapy commenced with PF-03732010, a humanized anti-*CDH3* monoclonal antibody (mAb) with demonstrated antitumor activity confirmed by carcinoma mouse models [6]. More recently, a clinical trial (ClinicalTrials.gov accession no. NCT00557505) revealed that this antibody was well tolerated in humans but demonstrated no significant anti-tumor activity in solid tumors to warrant further development as a naked antibody [7]. Nonetheless, due to the favorable toxicity profile of the anti-*CDH3* antibody and the interesting features of the target molecule, a radioimmunotherapy approach was proposed to achieve enhanced anti-tumor activity. The method of conjugating targeting antibodies or peptides with radionuclides has been successful in treating well-differentiated neuroendocrine tumors, prostate cancer, and other cancers [8–10]. Since high accumulation and homogeneous distribution at the target site and rapid elimination from non-target tissues are desirable for radiopharmaceutical therapy (RPT), the half-life of the radionuclide should be long enough to allow the radiolabeled monoclonal antibody (or peptide) to reach the tumor, and short enough to limit radiation exposure to normal tissues [11]. In addition, the specificity of the selected antibody to the cellular target enables increased therapeutic efficacy while minimizing toxicity to normal tissues [12–15].

FF-21101, a human–mouse chimeric immunoglobulin G1 (IgG1) monoclonal antibody (mAb) targeting human P-cadherin is being developed as a radio-immuno-therapeutic (RIT) for the treatment of patients with advanced solid tumors. In this paper, we describe FF-21101 as the mAb conjugate to the polydentate macrocyclic ligand, 1,4,7,10-tetraazacyclododecane-1,4,7,10-tetraacetic acid (DOTA) for use in dosimetry, imaging (e.g., with ^{111}In), or as a radioimmunotherapeutic (e.g., with ^{90}Y). The DOTA chelator forms stable metal complexes with a number of divalent and trivalent metals, including the lanthanide, indium-111 (^{111}In) [16].

Tumor geometry is considered to be a significant variable for the success of RIT, and it has been proposed that the emission characteristics of the radionuclide should be matched appropriately to the lesion size/volume to be treated in order to focus energy within the tumor rather than in the surrounding tissues [17]. Therefore, for our study, FF-21101 was labeled with the theranostic pair, ^{111}In and ^{90}Y . The nuclear properties of ^{111}In (physical half-life of 67.3 h and decay via electron capture with gamma emissions of 172 and 245 keV to stable cadmium-111) are well suited for multi-day imaging studies using planar gamma camera imaging and single photon emission computed tomography (SPECT). These nuclear properties are well matched with the 64.1 h physical half-life of yttrium-90 (^{90}Y) and the biological half-life of the IgG form of the FF-21101 product [18]. ^{90}Y emits beta particles, which penetrate soft tissue to a relatively long spatial depth of 5.3 mm. Therefore, ^{90}Y -labeled mAbs cause DNA damage to the targeted cells as well as to adjacent or more distant cells due to their long range [19]. As a result of this cross-fire effect, there is an

expectation that FF-21101(^{90}Y) will have a more positive therapeutic impact on treating solid tumors than anti-CDH3 therapies alone, making ^{90}Y ideal for this purpose [20]. ^{90}Y is also used clinically for radioembolization of hepatocellular carcinoma and metastatic disease to the liver from colon cancer using microspheres [21]. Unfortunately, while ^{90}Y has a favorable characteristic as a therapeutic radionuclide, the lack of gamma emission makes it suboptimal for imaging and dosimetry and dictates the need to delineate its biodistribution with a γ -emitting surrogate [22,23]. ^{111}In has, therefore, been the surrogate radionuclide of choice for ^{90}Y for gamma camera imaging due to the similarities in metabolic handling [24] and coordination chemistry with ^{90}Y [25,26].

In this study, we evaluated the biodistribution and dosimetry of FF-21101(^{111}In) in cynomolgus macaques. We estimated human adult male and female organ radiation absorbed doses by computing non-human primate (NHP) residence times based on serial gamma camera imaging and mass-scaled them to estimate the human equivalents. This was followed by the calculation of human absorbed dose estimates according to the methodology developed by the Medical Internal Radiation Dose (MIRD) Committee [18]. In order to compute internal radiation dose estimates for FF-21101(^{90}Y) for radioimmunotherapy, ^{111}In residence times obtained from FF-21101(^{111}In) were converted to ^{90}Y equivalents.

2. Material and Methods

2.1. Radiolabeling Preparation of FF-21101(^{111}In)

The monoclonal antibody (FF-21101) conjugated to DOTA was provided as a 5 mg/mL solution in 250 mM sodium acetate, pH 5.5, by FUJIFILM Diosynth Biotechnologies, USA, Inc., Morrisville, NC, USA. Indium-111 chloride ($^{111}\text{InCl}_3$) was purchased from Mallinckrodt, Inc., St. Louis, MO, USA, and stored securely according to manufacturer specifications until ready for use. A preset volume of FF-21101 was transferred to a sterile 10 mL reaction vial (Greer Laboratories, Lenoir, NC, USA) using aseptic techniques and mixed with $^{111}\text{InCl}_3$ in a shielded laminar air flow hood; the specific radioactivity of the mixture was 37 MBq/mg at the time of injection. The radioactive dose volume at the time of preparation was calculated based on the radioactive concentration of $^{111}\text{InCl}_3$ at the time of preparation and added to the reaction vial. The reaction mixture was incubated at 40 °C in a thermomixer for 20 min. Following incubation, clinical formulation buffer (25 mmol/mL sodium acetate, 2 mg/mL ascorbic acid, 0.3 mg/mL diethylene triamine pentaacetic acid, and 0.72% saline; AMRI, Burlington, MA, USA) was added to bring the total volume to 10 mL. Approximately 111 MBq of FF-21101(^{111}In) in 5 mL was drawn from the reaction vial into a pre-labeled 10 mL syringe, assayed in a dose calibrator, and delivered for injection. Labeled antibody was purified using a Biospin Column 6 (Bio-Rad, Tokyo, Japan) according to the manufacturer's instructions. The labeling processes did not result in degradation of these antibodies.

2.2. Determination of Specific Activity

The specific activity of FF-21101(^{111}In) was calculated based on measurements of radioactivity concentration and molar concentration in the dosing injectate. The radioactivity concentration of FF-21101(^{111}In) was determined using a Packard 5500 gamma spectrometer (Perkin-Elmer, Waltham, MA, USA).

2.3. Experimental Animals

After a five-week quarantine/acclimation period, six adult (3 male and 3 female) cynomolgus macaques were housed separately in a facility accredited by the Association for Assessment and Accreditation of Laboratory Animal Care International. All experiments were performed following published guidelines under a protocol approved by the Institutional Animal Care and Use Committee. Prior to imaging, the animals were fasted overnight but had free access to water. The animals were anesthetized with an intramuscular injection of ketamine (10–15 mg/kg) plus atropine sulfate (0.04 mg/kg) to facilitate tracheal intubation. Anesthesia was maintained via inhalation of isoflurane (1%

to 3%) and oxygen delivered by a Fabius Tiro gas anesthesia system (Dräger Medical, Inc., Tokyo, Japan). Cannulas were placed in both saphenous veins of each animal: one cannula was used for administration of the FF-21101 (^{111}In) and the other was used for repetitive blood sampling. Body temperature was maintained at 37 ± 0.8 °C using an air-circulating heating device (model 505; Arizant Healthcare Inc., Eden Prairie, MN, USA). The electrocardiogram, pulse oximetry, and respiration rates were continuously monitored using an Infinity Gamma XL Monitor (Dräger Medical, Inc.). The stage of menstrual cycle in females was not monitored. The use of a vacuum immobilization system bag was instrumental in helping to maintain NHP position throughout each planar/SPECT and subsequent CT scan imaging sessions over several days.

2.4. Gamma Camera and SPECT System

All animal whole-body (WB) planar and SPECT gamma camera imaging studies were performed using a Siemens Symbia S scanner (Siemens Medical Solutions USA, Hoffman Estates, IL, USA) equipped with two 3/8" NaI detectors and medium-energy low-penetration collimators. The reported NEMA ^{111}In system planar sensitivity for that system is 430 cpm/ μCi .

2.5. Gamma Camera and SPECT Imaging Protocol

Each primate was first placed in a vacuum immobilization bag to maintain consistent positioning during each planar/SPECT and CT imaging session. All primates were positioned supine/feet first into the gantry. Approximately 111 MBq of ^{111}In -FF-21101 was administered to each primate as a continuous infusion over 10 min. A (0 h) planar/SPECT scanning session commenced immediately after the end of the infusion and consisted of a head-to-foot whole-body planar sweep followed by either a single-bed (female) or two-bed (male), head-neck-trunk SPECT scan. This planar-plus-SPECT-imaging paradigm was repeated multiple times according to the following schedule: 2, 24, 48, 72, 96, and 120 h from the end of infusion. A 10 mL liquid vial ^{111}In calibration source (approximately 1.85 MBq) was acquired along with the NHP at each time point, to convert reconstructed SPECT counts to activity.

For whole-body planar imaging, the acquisition parameters were set as follows: a 256×1024 acquisition matrix, and a scan speed of 10 cm/min (0, 2, 24 h), 7 cm/min (48, 72 h), or 5 cm/min (96, 120 h), with 15% ($\pm 7.5\%$) energy window widths centered over the two ^{111}In photopeaks (172 and 245 keV). For SPECT imaging, the acquisition parameters were: 128 views over 360° (64 views/head and 180° total gantry rotation), 15 sec/view (0, 2, 24 h), 21 sec/view (48, 72 h), or 30 sec/view (96, 120 h). Images were acquired and reconstructed in a 128×128 matrix with a pixel size of 4.8 mm. In addition to the two photopeak images, images from a scatter window below the 245 keV photopeak (211 keV/11%) and scatter windows below and above the 172 keV photopeak (144 keV/18% and 190 keV/7%) were also acquired, for dual- and triple-energy-window scatter compensation, respectively. An ordered-subset expectation-maximum iterative algorithm (8 iterations, 16 subsets, and 9.6 mm full-width at half-maximum Gaussian post-filter), incorporating CT-based attenuation correction (AC) and energy-window-based scatter and system spatial resolution compensations, was employed for reconstruction of the SPECT images.

2.6. CT Imaging

The CT imaging was performed on a GE 750 HD scanner (General Electric Healthcare, Waukesha, WI, USA) and was used for SPECT attenuation correction and to help identify the contours of the source organ's volumes of interest (VOIs). Primates were positioned centrally on the CT scanner table. A scout scan (AP, 120 kVp, 80 mA, 100 cm, 10 cm/s) was first acquired to determine animal positioning and anatomical coverage. This was followed by a CT scan with the following parameters: 120 kVp, Smart mA tube current modulation, 0.5 s rotation, 64×0.625 mm nominal beam width at isocenter, and 1.375 pitch.

The AC CT-filtered back-projection reconstruction parameters were 5 mm slice thickness and spacing, 50 cm diameter, and STANDARD filter; while those for the organ-contouring CT were 3.75 mm slice thickness, 3.27 mm slice spacing, 50 cm diameter, and SOFT filter.

2.7. Image Analysis for Dosimetry Calculations

Three-dimensional VOIs of identifiable source organs of radioactivity were manually defined on the first-day CT scan and all serial SPECT scans were manually registered to that CT scan using MIM version 6.5 (MIM Software Inc., Beachwood, OH, USA). These VOIs were used for both CT-based organ mass estimation and SPECT organ activity versus time (time–activity curve, [TAC]) generation. The identifiable source organs were heart contents, lungs, liver, spleen, kidneys, and testes. Two-dimensional total-body regions of interest were defined in an analogous fashion using the planar whole-body scan images, for total-body TAC generation.

2.8. Blood Sampling

Measurement of radioactivity concentrations in the blood was based on 0.5 mL venous blood samples obtained via the catheterized vein at 1, 2, 5, 10, 15, 20, and 30 min, and 2, 24, 48, 72, 96, and 120 h after FF-21101(¹¹¹In) injection. Approximately 50 mg of each blood sample was assayed along with an ¹¹¹In counting standard, to derive radioactivity concentration versus time using a gamma counter (Cobra Quantum, Perkin-Elmer, Waltham, MA, USA), expressed as a Fraction of Injected Activity per mL (FIA/mL).

2.9. Residence Time and Absorbed Dose Calculations

Human organ radiation absorbed dose estimates for FF-21101(¹¹¹In) (mGy/MBq) were obtained using the MIRD methodology. The MIRD equation for estimating mGy/MBq to a target from one or more sources is

$$D_t = \sum_{i=1}^n T_s \times S_i(t \leftarrow s)$$

where D_t is the dose to a target (mGy/MBq); T_s is the residence time (or normalized cumulative activity, equal to the total number of disintegrations per unit of administered activity, in h) in source s ; and $S_i(t \leftarrow s)$ is the average absorbed dose in target t per unit of cumulative activity, \widetilde{A}_s , in source s (dose factor, in mGy/MBq-h). Cumulative activity and residence time T_s are related as follows:

$$\widetilde{A}_s = A_0 \times T, \text{ or equivalently, } T_s = \widetilde{A}_s / A_0$$

where A_0 is administered activity. Residence time was computed based on the imaging data acquired from all macaques as the fraction of administered activity in the source, $f_s(t)$, integrated from time $t = 0$ to ∞ . The dose factors employed in the dose calculations were those defined in the FDA-cleared and *de facto* industry-standard program OLINDA/EXM 1.1 (Vanderbilt University, Nashville, TN, USA). Human radiation doses were calculated from all cynomolgus macaques and the normalized number of disintegrations using OLINDA/EXM 1.1 for the adult male and female phantoms. Supplementary Materials describe the dosimetry assumptions in detail.

The calculated absorbed doses for FF-21101(¹¹¹In) and FF-21101(⁹⁰Y) were then compared with the published absorbed doses for ibritumomab tiuxetan (Zevalin; Acrotech Biopharma, LLC, East Windsor, NJ, USA) labeled with the same radionuclides (¹¹¹In and ⁹⁰Y) [18].

3. Results

3.1. FF-21101(¹¹¹In) Synthesis

Radiolabeling of FF-21101 with ¹¹¹InCl₃ was carried out by the clinical site radiopharmacy. The prescribed radiolabeled activities were assayed using a pre-calibrated dose calibrator, prepared in the empty reaction vial, drawn into an appropriately sized sterile

syringe, and sterile-filtered prior to infusion into the subject. Radiochemical purity of the product was assayed using radio-thin layer radiochromatography and typically exceeded 98% up to 24 h post-compounding. Each primate was administered 103.6–189.8 MBq of FF-21101(^{111}In) in a volume of 5 mL. FF-21101 antibody concentration administered to each animal ranged from 0.48 to 0.54 mg/mL. Antibody dose ranged from 0.29 to 0.63 mg/kg (mean of 0.34 mg/kg for males and mean of 0.59 mg/kg for females). Simultaneously, with the FF-21101(^{111}In) injection, up to 15 mL of saline was infused using a second syringe through the same catheter port; this infusion of saline was continued for ~30 s after the end of the FF-21101(^{111}In) administration to steadily flush the infusion line.

3.2. Planar/SPECT Imaging of FF-21101(^{111}In)

FF-21101(^{111}In) accumulated in the spleen, lungs, liver, kidneys, and heart contents in all six primates (Figure 1A). It is noteworthy that the testes of the male NHPs were considered a source organ due to FF-21101(^{111}In)-specific accumulation being visible in the whole-body planar images. This necessitated a second bed position SPECT scan over the pelvic region to properly account for the radioactivity in the testes (Figure 1B). Due to the size of male NHPs, the axial extent of the first bed position SPECT scan only covered the head through to the mid-lower abdomen. In contrast, the ovaries of female NHPs did not show radiotracer accumulation above that of the surrounding body tissue, and, hence, were not considered as a source organ. As a result, only a single-bed position SPECT scan was required (Figure 1C). In addition, we have included a representative image of a female from the Phase-I clinical trial with an adenocarcinoma of the vagina, in which tumors surround the urinary bladder (Figure 1D). As a reference, subsequent FDG(^{18}F) PET imaging obtained as standard of care demonstrates increased radiotracer uptake localizing to the vaginal tumor that corresponded to the area of FF-21101(^{111}In) uptake (Figure 1E).

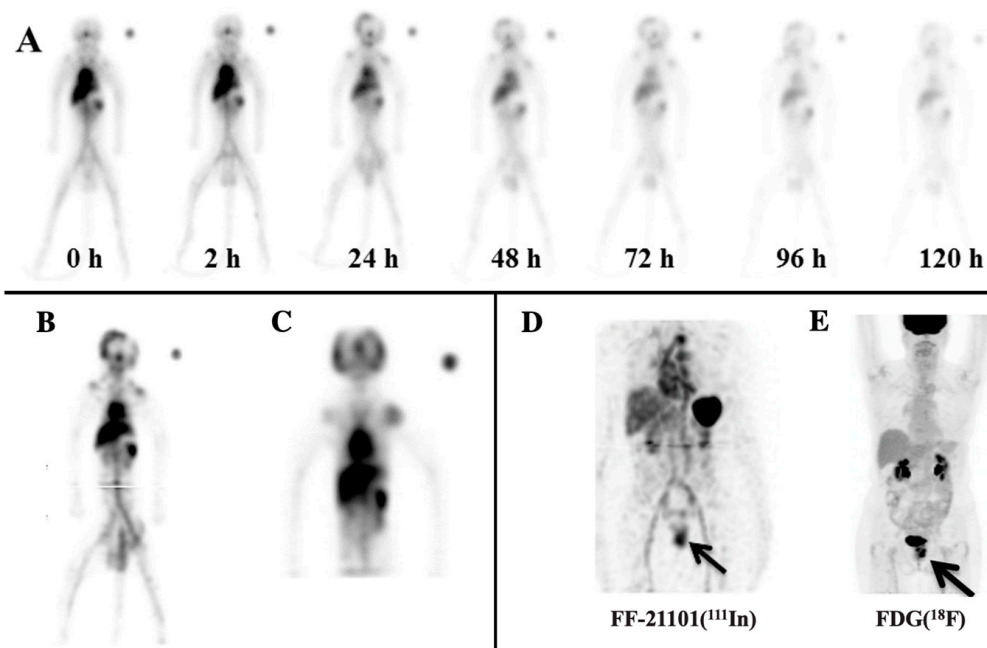


Figure 1. Representative NHP FF-21101(^{111}In) scans: (A) Male NHP anterior whole-body planar images (female biodistribution was the same, aside from the testes); (B) summed coronal view of the 24 h, two-bed SPECT of the same NHP male; and (C) summed coronal view of a female 24 h, single-bed SPECT. The scans demonstrate uptake in blood pool, lungs, liver, spleen, kidneys, and testes. (D) FF-21101(^{111}In) MIP SPECT image of a 69-year-old female with an adenocarcinoma of the vagina. A black arrow indicates that FF-21101(^{111}In) activity is increased in the recurrent tumor in the mid-to-lower left vaginal wall. (E) Subsequent MIP FDG(^{18}F) PET demonstrated high uptake within both urinary bladder and the uterine tumor, thus confirming the location of the adenocarcinoma of the vagina.

3.3. Pharmacokinetics of FF-21101(¹¹¹In)

The 0 to 120 h planar/SPECT imaging demonstrated that the hepatobiliary system was the primary route for clearance of FF-21101(¹¹¹In). Hence, despite accumulation in the kidneys, radiotracer activity in the urinary bladder activity was not prominent.

The time-dependent biologic FF-21101(¹¹¹In)-derived NHP FIA/mL in whole blood (Figure 2A) reached a mean peak value of 0.0037 ± 0.00093 standard error of the mean (SEM) within 2 h. Radioactivity counts decreased 40% mono-exponentially to a mean of 0.0022 ± 0.00042 SEM within 24 h after injection. At the end of the measurements, blood FIA/mL decreased by an average of 78% to a mean of 0.00079 ± 0.00016 SEM at 120 h. The corresponding time-dependent biologic FF-21101(¹¹¹In)-derived humanized FIA/mL in whole blood are presented in Figure 2B, following the same pattern of decrease in radioactivity.

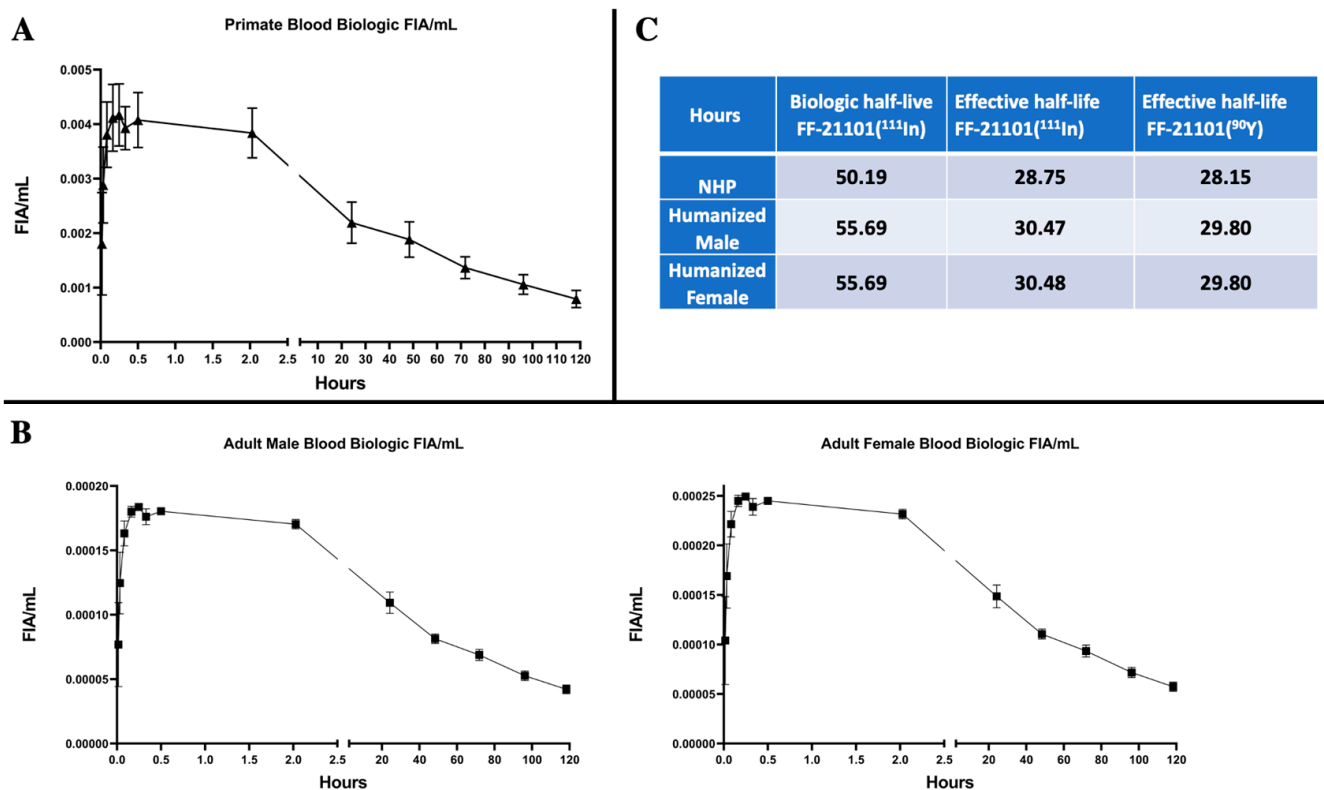


Figure 2. Primate (A) and Humanized (B) Biologic (decay-corrected) fraction of injected activity per mL (FIA/mL) of FF-21101(¹¹¹In) in the blood. Data points: Mean \pm SEM. Biologic and effective half-life (C) calculated from FIAs.

As expected, relatively low accumulation of FF-21101(¹¹¹In) was observed in most organs not involved in the biological clearance of FF-21101(¹¹¹In)-derived radioactivity (Figure 3). We did not observe retention or accumulation of FF-21101(¹¹¹In) in the brain.

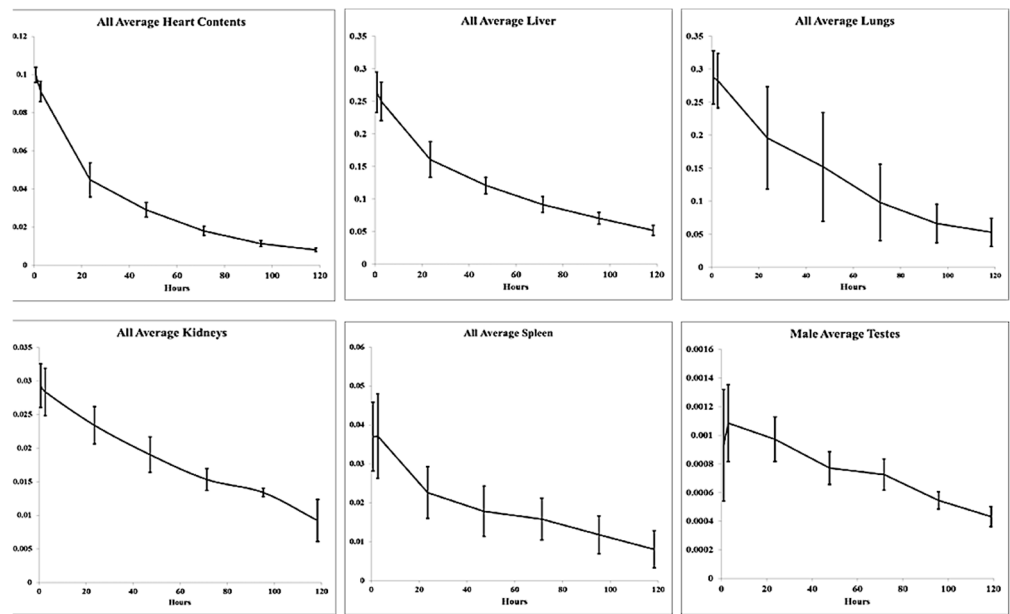


Figure 3. Humanized fraction of FF-21101(¹¹¹In) versus time in identified source organs. Data points: mean ± SD.

3.4. Radiation Dosimetry

Source organ residence times for FF-21101(¹¹¹In) and FF-21101(⁹⁰Y) are shown in Tables 1 and 2, respectively; the corresponding organ doses are shown in Tables 3 and 4.

Table 1. Humanized FF-21101(¹¹¹In) source organ residence times (h) for the derived from NHP dosimetric data.

Source Organ	FF-21101(¹¹¹ In) Residence Time (h)				¹¹¹ In-Ibritumomab Tiuxetan Human Published: [18]			
	Overall		Females		Males		Published: [18]	
	Mean	Std Dev	Mean	Std Dev	Mean	Std Dev	Mean	Std Dev
Heart Contents	3.845	0.302	3.828	0.342	3.857	0.351	1.18	0.557
Kidneys	3.412	0.566	3.556	1.095	3.316	0.082	1.4	0.351
Liver	16.414	2.194	15.914	0.529	16.747	3.012	12.9	4.92
Lungs	15.407	2.792	13.53	1.471	16.658	2.938	1.41	0.904
Spleen	3.101	0.89	2.256	0.19	3.664	0.613	1.63	0.814
Red Marrow	3.085	0.837	3.995	0.103	2.477	0.114	11.7	4.52
Testes	0.151	0.019	NA	NA	0.151	0.019	0.163	0.065
Total Body	84.828	2.905	82.191	2.627	86.585	1.357	82.183	2.062
Remainder of Body	39.473	5.467	39.112	3.109	39.714	7.398	51.8	16.2

Table 2. Humanized FF-21101(⁹⁰Y) source organ residence times (h) derived from those for FF-21101(¹¹¹In).

Source Organ	FF-21101(⁹⁰ Y) Residence Time (h)					
	Overall		Females		Males	
	Mean	Std Dev	Mean	Std Dev	Mean	Std Dev
Heart Contents	3.768	0.293	3.654	0.286	3.781	0.340
Kidneys	3.209	0.494	3.319	0.678	3.128	0.069
Liver	15.874	2.109	16.518	2.036	16.219	2.890
Lungs	14.98	2.686	18.603	9.426	16.171	2.839
Spleen	2.972	0.838	1.843	0.573	3.510	0.550
Red Marrow	3.028	0.818	4.300	0.665	2.434	0.110
Testes	0.142	0.018	NA	NA	0.142	0.018
Total Body	81.253	2.689	80.591	3.533	82.885	1.247
Remainder of Body	37.339	5.237	32.354	8.500	37.499	7.071

Table 3. OLINDA/EXM 1.1 organ radiation absorbed dose estimates for FF-21101(¹¹¹In).

Organ	Female		Male				¹¹¹ In-Ibritumomab Tiuxetan Human Published [18]	
	Average mSv/MBq	Std Dev mSv/MBq	Average mSv/MBq	Std Dev mSv/MBq	Average mSv/MBq	Std Dev mSv/MBq	Average mSv/MBq	Std Dev mSv/MBq
Adrenals	0.310	0.028	0.251	0.011	0.281	0.037	0.202	0.041
Brain	0.067	0.013	0.059	0.010	0.063	0.011	0.082	0.020
Breasts	0.136	0.018	0.113	0.003	0.124	0.017	0.080	0.016
Gallbladder Wall	0.317	0.019	0.268	0.020	0.293	0.032	0.229	0.059
LLI Wall	0.105	0.018	0.090	0.013	0.098	0.017	0.130	0.027
Small Intestine	0.130	0.014	0.118	0.010	0.124	0.013	0.145	0.027
Stomach Wall	0.189	0.004	0.164	0.005	0.176	0.014	0.139	0.028
ULI Wall	0.152	0.014	0.128	0.008	0.140	0.016	0.147	0.027
Heart Wall	0.498	0.046	0.403	0.025	0.451	0.061	0.195	0.048
Kidneys	0.671	0.114	0.586	0.008	0.629	0.086	0.315	0.071
Liver	0.851	0.112	0.650	0.100	0.751	0.145	0.467	0.202
Lungs	0.999	0.445	0.681	0.101	0.840	0.337	0.152	0.036
Muscle	0.124	0.004	0.104	0.005	0.114	0.012	0.103	0.021
Ovaries	0.112	0.018	NA	NA	0.112	0.018	0.138	0.028
Pancreas	0.290	0.009	0.257	0.012	0.274	0.020	0.199	0.041
Red Marrow	0.181	0.012	0.145	0.005	0.163	0.022	0.272	0.065
Osteogenic Cells	0.276	0.012	0.218	0.019	0.247	0.035	0.312	0.050
Skin	0.068	0.005	0.060	0.005	0.064	0.006	0.065	0.015
Spleen	0.675	0.150	0.958	0.140	0.816	0.202	0.464	0.193
Thymus	0.197	0.022	0.167	0.012	0.182	0.023	0.114	0.024
Thyroid	0.095	0.003	0.141	0.038	0.118	0.035	0.098	0.024
Urinary Bladder Wall	0.089	0.018	0.087	0.010	0.088	0.013	0.113	0.028
Uterus	0.107	0.019	NA	NA	0.107	0.019	0.132	0.029
Testes	NA	NA	0.114	0.044	0.114	0.044	0.175	0.076
Total Body	0.162	0.009	0.133	0.002	0.148	0.017	0.124	0.022
Effective Dose Eq	0.382	0.054	0.339	0.023	0.360	0.044		
Effective Dose	0.279	0.050	0.241	0.015	0.260	0.039		

The median biologic half-life for the circulating antibody in whole blood of NHPs was 50.19 h with a median effective half-life of 28.75 h for FF-21101(¹¹¹In). The corresponding median effective half-life for FF-21101(⁹⁰Y) in NHPs was 28.15 h. In comparison, the derived humanized median biologic half-life of FF-21101(¹¹¹In) was 55.69 h with an effective half-life of 29.8 h for FF-21101(⁹⁰Y) (Figure 2C).

Although OLINDA/EXM 1.1 computes the equivalent dose (mSv/MBq), the radiation weighting factors for all the emissions (photon and electron) from ¹¹¹In and ⁹⁰Y are in unity, thus, the equivalent dose is the same as the radiation absorbed dose for both, i.e., 1 mSv = 1 mGy. The results are tabulated for a reference adult human (male and female). In each case, a comparison with the published absorbed doses for ibritumomab tiuxetan labeled with the same radionuclide is also provided [18]. The organs with the five-highest estimated absorbed doses for FF-21101(¹¹¹In) were the lungs (0.840 mSv/MBq), spleen (0.816 mSv/MBq), liver (0.751 mSv/MBq), kidneys (0.629 mSv/MBq), and heart wall (0.451 mSv/MBq). The organs with the five-highest estimated absorbed doses for FF-21101(⁹⁰Y) were similar to those for FF-21101(¹¹¹In): lungs (10.49 mSv/MBq), spleen (8.21 mSv/MBq), kidneys (5.92 mSv/MBq), liver (5.46 mSv/MBq), and heart wall (2.61 mSv/MBq). Comparison between the male and female dose estimates shows similar organ doses, as well as the ¹¹¹In effective dose, suggesting similar biodistribution profiles for the two genders. Similar trends were observed in human dosimetry for ¹¹¹In/⁹⁰Y-ibritumomab tiuxetan (Tables 3 and 4). For all NHPs, the humanized estimates for FF-21101(⁹⁰Y)-administered activity were below the applicable limits for external beam radio-

therapy (<3 Gy to red marrow, <30 Gy to the liver, and <20 Gy to the kidneys and lungs, <1 Gy to the testes, <2 Gy to the ovaries) [27,28].

Table 4. OLINDA/EXM 1.1 organ radiation absorbed dose estimates for FF-21101(⁹⁰Y).

Organ	Female		Male				⁹⁰ Y-Ibritumomab Tiuxetan Human Published [18]	
	Average mSv/MBq	Std Dev mSv/MBq	Average mSv/MBq	Std Dev mSv/MBq	Average mSv/MBq	Std Dev mSv/MBq	Average mSv/MBq	Std Dev mSv/MBq
Adrenals	0.306	0.081	0.274	0.052	0.290	0.063	0.379	0.118
Brain	0.306	0.081	0.274	0.052	0.290	0.063	0.379	0.118
Breasts	0.306	0.081	0.274	0.052	0.290	0.063	0.379	0.118
Gallbladder Wall	0.306	0.081	0.274	0.052	0.290	0.063	0.379	0.118
LLI Wall	0.306	0.081	0.274	0.052	0.290	0.063	0.379	0.118
Small Intestine	0.306	0.081	0.274	0.052	0.290	0.063	0.379	0.118
Stomach Wall	0.306	0.081	0.274	0.052	0.290	0.063	0.379	0.118
ULI Wall	0.306	0.081	0.274	0.052	0.290	0.063	0.379	0.118
Heart Wall	2.707	0.231	2.513	0.190	2.610	0.217	1.080	0.394
Kidneys	6.333	1.296	5.497	0.119	5.915	0.942	2.440	0.610
Liver	6.353	0.785	4.573	0.817	5.463	1.210	3.640	1.389
Lungs	12.277	6.206	8.710	1.528	10.493	4.489	0.761	0.488
Muscle	0.306	0.081	0.274	0.052	0.290	0.063	0.379	0.118
Ovaries	0.306	0.081	NA	NA	0.306	0.081	0.379	0.118
Pancreas	0.306	0.081	0.274	0.052	0.290	0.063	0.379	0.118
Red Marrow	1.008	0.071	0.705	0.053	0.857	0.175	2.730	0.909
Osteogenic Cells	1.283	0.023	0.742	0.087	1.013	0.302	2.140	0.519
Skin	0.306	0.081	0.274	0.052	0.290	0.063	0.379	0.118
Spleen	6.41	1.989	10.010	1.552	8.210	2.536	4.650	2.327
Thymus	0.306	0.081	0.274	0.052	0.290	0.063	0.379	0.118
Thyroid	0.306	0.081	0.274	0.052	0.290	0.063	0.379	0.118
Urinary Bladder Wall	0.306	0.081	0.274	0.052	0.290	0.063	0.379	0.118
Uterus	0.306	0.081	NA	NA	0.306	0.081	0.379	0.118
Testes	NA	NA	1.860	0.233	1.860	0.233	2.160	0.842
Total Body	0.738	0.035	0.588	0.010	0.663	0.086	0.587	0.107

4. Discussion

Radioimmunotherapy and peptide receptor radionuclide therapy are both unique approaches for the targeting and treatment of tumors with a high degree of specificity. Both approaches offer great promise to deliver a lethal dose of radiation to cancer cells while significantly reducing the radiation dose to normal organs. Compounds that have been shown to have such favorable therapeutic abilities and safety profiles are ⁹⁰Y-ibritumomab tiuxetan (as an example for radioimmunotherapy) and ¹⁷⁷Lu-DOTATATE (Lutathera, Advanced Accelerator Application, USA, Inc., Millburn, NJ, USA, as an example of peptide receptor radionuclide therapy) [29]. FF-21101 is a human–mouse chimeric immunoglobulin of the IgG1 subclass that targets human P-cadherin and may prove to be another successful therapeutic agent for radioimmunotherapy applications.

This study provides information on non-target uptake levels of FF-21101(¹¹¹In/⁹⁰Y) in normal organs and was conducted to facilitate a Phase I clinical trial with FF-21101 radiolabeled with ¹¹¹In for dosimetry and ⁹⁰Y for therapy. All animals tolerated the imaging procedures and intravenous infusion of FF-21101(¹¹¹In) well, with minimal discomfort. The use of the immobilizer was instrumental and helped in the fusion alignment of the planar (WB) and SPECT images, and, thus, decreased the possibility of significant errors due to organ volume contouring or dose calculation errors because of image misregistration. No significant weight loss was observed in the animals. Biodistribution and radiation dosimetry were evaluated after intravenous infusion of FF-21101(¹¹¹In) in six cynomolgus macaques, with an activity range of 103.6–189.8 MBq. The radiation absorbed doses were

increased in organs affected by blood flow. The source organs identified by FF-21101(^{111}In) in decreasing order by dose were the lungs, spleen, liver, kidneys, and heart wall; and for FF-21101(^{90}Y), the lungs, spleen, kidneys, liver, and heart wall. The amount of FF-21101(^{111}In) that was associated with the ovaries and testes was similar, given that most of its dose came from surrounding source organs; however, since the testes are in fact source organs (whereas ovaries are not), the dose absorbed by testes from FF-21101(^{90}Y) is much higher (1.86 in testes vs. 0.306 mSv/MBq in ovaries), as ^{90}Y is a pure beta emitter. Thus, it is important to evaluate the dosimetry profile of animal models in both genders.

The FDA package insert specifies an effective half-life of 30 h for ^{90}Y -ibritumomab tiuxetan, which is in agreement with our calculations [30]. The pattern of biodistribution and clearance of FF-21101(^{111}In) in NHPs was similar to that reported in humans for ^{111}In -ibritumomab tiuxetan [18]. All source organs exhibited uptake and mono-exponential clearance typical of an intact mAb, with the five-highest absorbed dose estimates (D) (mSv/MBq) of FF-21101(^{111}In) in the lungs, spleen, liver, kidneys, and heart wall. The order of organs with the five-highest absorbed D values in the ^{111}In -ibritumomab tiuxetan studies was slightly different, with the highest exposure to the liver, spleen, kidneys, osteogenic cells, and red marrow. The radiation absorbed dose from ^{90}Y -ibritumomab tiuxetan in the lungs was low in comparison to FF-21101(^{90}Y) (0.761 and 10.495 mSv/MBq, respectively). The spleen was shown to have the highest absorbed radiation dose from ^{90}Y -ibritumomab tiuxetan, yet the dose from FF-21101(^{90}Y) was double that of the spleen. The doses to the kidneys and liver followed a similar pattern to that of the spleen. The dose from FF-21101(^{90}Y) in red marrow was significantly lower than that of ^{90}Y -ibritumomab tiuxetan (0.857 vs. 2.73 mSv/MBq, respectively). The difference in absorbed D values is not unexpected given the mechanism of action of ibritumomab (anti-CD20) versus FF-21101 (anti-P-cadherin). ^{111}In -ibritumomab tiuxetan is an immunoconjugate of a murine anti-CD20 mAb approved in 2002 by the FDA for assessing its biodistribution in low-grade or follicular B-cell non-Hodgkin's lymphoma patients prior to ^{90}Y -ibritumomab tiuxetan (Zevalin[®]) therapy [31].

In RPT, tumor cell killing is achieved by delivering ionizing radiation [32]. In our case, we used ^{90}Y for the therapeutic component. This radionuclide emits high-energy beta particles (2300 keV maximum beta energy ($E_{\beta\text{max}}$)), with 90% of its energy being absorbed within a sphere corresponding to 100–200 cell diameters. This gives ^{90}Y a broad crossfire effect locally, which is ideal for treating solid tumors [20]. The favorable imaging and dosimetry results of this study further support the possibility of exploring the integration of FF-21101 in future clinical trials. One such Phase I study has already been conducted at the MD Anderson Cancer Center (ClinicalTrials.gov Identifier: NCT02454010) to investigate a number of parameters, including the determination of radiation dose estimates prior to radioimmunotherapy, its human biodistribution properties, and dosimetry profiles in primary solid tumors and metastases [33].

Table 5 compares humanized NHP organ radiation absorbed dose estimates for FF-21101(^{90}Y) to reported human-normalized FF-21101(^{90}Y) organ radiation absorbed dose estimates based on FF-21101(^{111}I) dosimetric imaging reported by Subbiah et al. from a Phase I clinical trial [33]. The NHP values in this table are reported in mGy/mCi to match the units of the published human dose estimates. The table shows that most organ dose estimates correlate relatively well within acceptable uncertainties. The difference between NHP and human values for kidneys, liver, red marrow, and osteogenic cells were all within less than 30% of each other. It was previously reported that the degree of uncertainty associated with the dosimetry data in human and preclinical studies was about 20–47% [34–36]. The biggest discrepancies in dose estimates are noted for the spleen, testes, and lungs. Several reasons could be attributed to these discrepancies. For example, the difference in the estimated spleen dose could be attributed to the differences in the subject population between the two studies. For the patient studies, human data were obtained from 16 patients (7 male and 9 female) with *advanced* solid tumors, while the data from the NHP were acquired from 6 *healthy* subjects. Subbiah et al. [33] reported P-

cadherin expression in tumors and normal tissues and demonstrated a moderate amount of P-cadherin expression in normal splenic tissue; however, as previously reported by others, nonspecific binding of mAbs as well as macrophage uptake [37,38] may cause increased tracer accumulation in the spleen, in addition to possible aggregation/complexation, which, when combined with patient tumor burden, may explain the 70% higher spleen human dose estimates. The difference in testicular values between the NHP and the human study, on the other hand, could be due to the size of cynomolgus macaques' testes in comparison to human testes. To delineate the ROIs in NHP, testes present several challenges due to their small size and resultant coarse images that lead to increased partial volume effects, thereby potentially causing the observed difference in dose estimates. Finally, the difference in observed lung dose estimates between the NHP and human study (129%) could be attributed to the effects of placing the primate in a vacuum immobilization bag to maintain consistent positioning during each planar/SPECT- and CT-imaging session. The tracheal intubation and administration of anesthesia could cause the increase in radiotracer accumulation in the lungs due to potential atelectasis of the lung.

Table 5. Humanized OLINDA/EXM 1.1 organ radiation absorbed dose estimates for FF-21101(⁹⁰Y) compared to reported human-normalized FF-21101(⁹⁰Y) organ radiation absorbed dose estimates based on FF-21101(¹¹¹I) dosimetric imaging.

Organ	Human Average (mGy/mCi) *	Std Dev	Primate Average (mGy/mCi) **	Std Dev	% Change
Spleen	1031.5	399.9	303.77	93.83	70.55
Testes	339.5	122.6	68.82	8.62	79.73
Kidneys	219.7	75.8	218.86	34.85	0.38
Lungs	168.9	56.9	388.24	166.09	129.86
Liver	160.6	58.5	202.13	44.77	25.86
Heart Wall	89.7	18.1	96.57	8.03	7.66
Osteogenic Cells	34.7	13.2	37.48	11.17	8.01
Red Marrow	29.6	11	31.71	6.48	7.13
Total Body	25.7	2.6	24.53	3.18	4.55
Ovaries	14.6	4.3	11.32	3.00	22.45
Uterus	14.6	4.3	11.32	3.00	22.45
All other organs	12.5	5.1	10.73	2.33	14.16

* Normalized average values of total dose estimates from 16 patients (7 male, 9 female) with advanced solid tumors refractory to or relapsed from prior therapy, as reported in Subbiah et al. [33]. ** Humanized average (mean) organ absorbed dose estimated and normalized from 6 healthy non-human primates (3 male, 3 female), reported as mSv/MBq in Table 4, and recalculated to mGy/mCi for comparison purposes.

5. Conclusions

Overexpression of P-cadherin in several types of tumors provides an attractive target for RIT [4,5]. The biodistribution and radiation dosimetry characteristics of FF-21101(¹¹¹In), as determined in NHPs, indicate that the radiation dose of this radiotracer to potential human patients is similar to that of other mAb-based agents used for planar and SPECT imaging (e.g., ibritumomab tiuxetan). The highest radiation dose is delivered to the lungs, followed by the spleen, liver, kidneys, and heart wall but all are within acceptable ranges. However, in this study, we assess that NHP internal dosimetry underestimated the radiation dose estimated in humans by 70% in the spleen and testes and overestimated the dose estimates in the lungs. Yet, the comparison of results in other organs between NHP and human data may be justified, despite differences in the acquisition parameters in tumor-bearing vs. healthy NHP subjects. Taken together, the results of this study confirm that

FF-21101 conjugated to ^{111}In for imaging and to ^{90}Y for radioimmunotherapy can be safely translated to clinical trials.

Supplementary Materials: The following supporting information can be downloaded at: <https://www.mdpi.com/article/10.3390/cancers15184532/s1>. References [39–41] are cited in the Supplementary Materials.

Author Contributions: Conceptualization, G.R., W.E., L.D.P., J.M. and O.M.; Methodology, G.R., W.E., V.S., J.M., A.P.M., J.G. and O.M.; Formal analysis, W.E., L.M. and O.M.; Investigation, V.S.; Data curation, V.P., A.P.M. and J.G.; Writing—original draft, G.R., W.E. and L.M.; Writing—review & editing, G.R., L.D.P., L.M. and O.M.; Visualization, L.M.; Supervision, G.R., V.S. and O.M.; Project administration, L.D.P. All authors have read and agreed to the published version of the manuscript.

Funding: Research support for this study was provided by FUJIFILM Pharmaceuticals USA., Inc., Cambridge, MA, USA.

Institutional Review Board Statement: The animal study protocol was approved by the Institutional Animal Care and Use Committee of the University of Texas MD Anderson Cancer (protocol number 2015-0220), Houston, TX, USA.

Informed Consent Statement: The image of a patient depicted on this manuscript was sourced from a clinical trial conducted at the University of Texas MD Anderson Cancer Center under the approval of the local Institutional Review Board. The specific written informed consent utilized on this clinical trial addresses the utilization of deanonymized images for publication purposes.

Data Availability Statement: The data presented in this study is available upon request from the corresponding author.

Acknowledgments: The authors would like to thank Masahiko Tokura for providing assistance during the execution of the experiments. We express our gratitude to Aaron Cherry, Adina Feldman, Jennifer Miller, Lisa Moore, and Dana Toomey for their technical assistance.

Conflicts of Interest: G. Ravizzini reports grants from FUJIFILM Pharmaceuticals U.S.A., Inc., during the conduct of the study as well as grants from Blue Earth Diagnostics, Inc. (U.S.A.), ABX GmbH, Alfasigma S.p.A., Novartis, Bayer, Amgen, Regeneron Pharmaceuticals Inc, Curium, and Clarity outside the submitted work. W.D. Erwin reports grants from FUJIFILM Pharmaceuticals U.S.A. during the conduct of the study, as well as grants from Oncosil Medical, Ltd., Ipsen Pharma SAS, and Alfasigma S.p.A. outside the submitted work. V. Subbiah reports grants from FUJIFILM Pharmaceuticals U.S.A., Inc., (clinical trials research support) during the conduct of the study; grants from FUJIFILM Pharmaceuticals U.S.A. outside the submitted work; research funding/grant support for clinical trials from Roche/Genentech, Novartis, Bayer, GlaxoSmithKline, Nanocarrier, Vegenics, Northwest Biotherapeutics, Berghealth, Incyte, Pharmamar, D3, Pfizer, Multivir, Amgen, Abbvie, Alfasigma, Agensys, Boston Biomedical, Idera Pharma, Inhibrx, Exelixis, Blueprint Medicines, Loxo Oncology, Medimmune, Altum, Dragonfly Therapeutics, Takeda, National Comprehensive Cancer Network, NCI-CTEP, UT MD Anderson Cancer Center, Turning Point Therapeutics, and Boston Pharmaceuticals; travel support from Novartis, Pharmamar, ASCO, ESMO, Helsinn, and Incyte; consultancy/advisory board relationships with Helsinn, Loxo Oncology/Eli Lilly, R-Pharma US, Incyte, QED Pharma, Medimmune, Novartis, and Signant Health; and other from Medscape. A. McCoy and J. Gonzalez report other from FUJIFILM Pharmaceuticals U.S.A. during the conduct of the study. O. Mawlawi reports grants from FUJIFILM Pharmaceuticals U.S.A. during the conduct of the study. No potential conflicts of interest were disclosed by the other authors.

References

1. Conacci-Sorrell, M.E.; Ben-Yedidia, T. Nr-CAM is a target gene of the beta-catenin/LEF-1 pathway in melanoma and colon cancer and its expression enhances motility and confers tumorigenesis. *Genes Dev.* **2002**, *16*, 2058–2072. [[CrossRef](#)] [[PubMed](#)]
2. Takeichi, M. The cadherins: Cell-cell adhesion molecules controlling animal morphogenesis. *Development* **1988**, *102*, 639–655. [[CrossRef](#)] [[PubMed](#)]
3. Shimoyama, Y.; Hirohashi, S. Cadherin cell-adhesion molecules in human epithelial tissues and carcinomas. *Cancer Res.* **1989**, *49*, 2128–2133. [[PubMed](#)]
4. Gamallo, C.; Moreno-Bueno, G. The prognostic significance of P-cadherin in infiltrating ductal breast carcinoma. *Mod. Pathol.* **2001**, *14*, 650–654. [[CrossRef](#)]

5. Stefansson, I.M.; Salvesen, H.B. Prognostic impact of alterations in P-cadherin expression and related cell adhesion markers in endometrial cancer. *J. Clin. Oncol.* **2004**, *22*, 1242–1252. [[CrossRef](#)]
6. Zhang, C.C.; Yan, Z. PF-03732010: A fully human monoclonal antibody against P-cadherin with antitumor and antimetastatic activity. *Clin. Cancer Res.* **2010**, *16*, 5177–5188. [[CrossRef](#)]
7. A Study of PF-03732010 in Patients with Advanced Solid Tumors. ClinicalTrials.gov ID NCT00557505. Available online: <https://clinicaltrials.gov/study/NCT00557505?tab=results> (accessed on 21 June 2023).
8. Strosberg, J.; Krenning, E. 177Lu-Dotatate for Midgut Neuroendocrine Tumors. *N. Engl. J. Med.* **2017**, *376*, 1391–1392. [[CrossRef](#)]
9. Hofman, M.S.; Violet, J. [(177)Lu]-PSMA-617 radionuclide treatment in patients with metastatic castration-resistant prostate cancer (LuPSMA trial): A single-centre, single-arm, phase 2 study. *Lancet Oncol.* **2018**, *19*, 825–833. [[CrossRef](#)]
10. Emmanouilides, C.; Witzig, T.E. Safety and efficacy of yttrium-90 ibritumomab tiuxetan in older patients with non-Hodgkin's lymphoma. *Cancer Biother. Radiopharm.* **2007**, *22*, 684–691. [[CrossRef](#)]
11. Oriuchi, N.; Higuchi, T. Current status of cancer therapy with radiolabeled monoclonal antibody. *Ann. Nucl. Med.* **2005**, *19*, 355–365. [[CrossRef](#)]
12. Basch, E. Toward patient-centered drug development in oncology. *N. Engl. J. Med.* **2013**, *369*, 397–400. [[CrossRef](#)] [[PubMed](#)]
13. Stokke, C.; Gabina, P.M. Dosimetry-based treatment planning for molecular radiotherapy: A summary of the 2017 report from the Internal Dosimetry Task Force. *EJNMMI Phys.* **2017**, *4*, 27. [[CrossRef](#)] [[PubMed](#)]
14. Vilgrain, V.; Pereira, H. Efficacy and safety of selective internal radiotherapy with yttrium-90 resin microspheres compared with sorafenib in locally advanced and inoperable hepatocellular carcinoma (SARAH): An open-label randomised controlled phase 3 trial. *Lancet Oncol.* **2017**, *18*, 1624–1636. [[CrossRef](#)] [[PubMed](#)]
15. Bastiaannet, R.; van Roekel, C. First Evidence for a Dose-Response Relationship in Patients Treated with (166)Ho Radioembolization: A Prospective Study. *J. Nucl. Med.* **2020**, *61*, 608–612. [[CrossRef](#)]
16. Heppeler, A.; Froidevaux, S. Radiometal-labelled macrocyclic chelator-derivatized somatostatin analogue with superb tumour-targeting properties and potential for receptor mediated internal radiotherapy-mediated. *Chem. Eur. J.* **1999**, *5*, 1974–1981. [[CrossRef](#)]
17. O'Donoghue, J.A.; Bardies, M. Relationships between tumor size and curability for uniformly targeted therapy with beta-emitting radionuclides. *J. Nucl. Med.* **1995**, *36*, 1902–1909.
18. Fisher, D.R.; Shen, S. MIRD dose estimate report No. 20: Radiation absorbed-dose estimates for 111In- and 90Y-ibritumomab tiuxetan. *J. Nucl. Med.* **2009**, *50*, 644–652. [[CrossRef](#)]
19. Lehnert, M.; Ludwig, H. Update on the rational use of Y-ibritumomab tiuxetan in the treatment of follicular lymphoma. *Onco. Targets Ther.* **2009**, *2*, 199–208.
20. Howell, R.W.; Rao, D.V. Macroscopic dosimetry for radioimmunotherapy: Nonuniform activity distributions in solid tumors. *Med. Phys.* **1989**, *16*, 66–74. [[CrossRef](#)]
21. Murthy, R.; Kamat, P. Radioembolization of yttrium-90 microspheres for hepatic malignancy. *Semin. Interv. Radiol.* **2008**, *25*, 48–57. [[CrossRef](#)]
22. Camera, L.; Kinuya, S. Comparative biodistribution of indium- and yttrium-labeled B3 monoclonal antibody conjugated to either 2-(p-SCN-Bz)-6-methyl-DTPA (1B4M-DTPA) or 2-(p-SCN-Bz)-1,4,7,10-tetraazacyclododecane tetraacetic acid (2B-DOTA). *Eur. J. Nucl. Med.* **1994**, *21*, 640–646. [[CrossRef](#)] [[PubMed](#)]
23. Wright, C.L.; Zhang, J. Theranostic Imaging of Yttrium-90. *Biomed. Res. Int.* **2015**, *2015*, 481279. [[CrossRef](#)] [[PubMed](#)]
24. Naruki, Y.; Carrasquillo, J.A. Differential cellular catabolism of 111In, 90Y and 125I radiolabeled T101 anti-CD5 monoclonal antibody. *Int. J. Rad. Appl. Instrum. B.* **1990**, *17*, 201–207. [[CrossRef](#)] [[PubMed](#)]
25. Maecke, H.R.; Riesen, A. The molecular structure of indium-DTPA. *J. Nucl. Med.* **1989**, *30*, 1235–1239.
26. Adams, G.P.; Shaller, C.C. A single treatment of yttrium-90-labeled CHX-A''-C6.5 diabody inhibits the growth of established human tumor xenografts in immunodeficient mice. *Cancer Res.* **2004**, *64*, 6200–6206. [[CrossRef](#)]
27. Emami, B.; Lyman, J. Tolerance of normal tissue to therapeutic irradiation. *Int. J. Radiat. Oncol. Biol. Phys.* **1991**, *21*, 109–122. [[CrossRef](#)]
28. Rubin, P.; Casarett, G.W. Clinical radiation pathology as applied to curative radiotherapy. *Cancer* **1968**, *22*, 767–778. [[CrossRef](#)]
29. Hope, T.A.; Abbott, A. NANETS/SNMMI Procedure Standard for Somatostatin Receptor-Based Peptide Receptor Radionuclide Therapy with (177)Lu-DOTATATE. *J. Nucl. Med.* **2019**, *60*, 937–943. [[CrossRef](#)]
30. Tiuxetan, I. ZEVALINTM. 2001, USA/Package Insert/ZEVALIN. Available online: https://www.accessdata.fda.gov/drugsatfda_docs/label/2002/ibride021902lb.pdf (accessed on 27 April 2023).
31. FDA. First radiopharmaceutical for non-Hodgkin's lymphoma. *FDA Consum.* **2002**, *36*, 3. Available online: https://permanent.access.gpo.gov/lps1609/www.fda.gov/fdac/departs/2002/302_upd.html#lymphoma (accessed on 26 April 2023).
32. Sgouros, G.; Dewaraja, Y.K. Tumor Response to Radiopharmaceutical Therapies: The Knowns and the Unknowns. *J. Nucl. Med.* **2021**, *62* (Suppl. S3), 12S–22S.
33. Subbiah, V.; Erwin, W. Phase I Study of P-cadherin-targeted Radioimmunotherapy with (90)Y-FF-21101 Monoclonal Antibody in Solid Tumors. *Clin. Cancer Res.* **2020**, *26*, 5830–5842. [[CrossRef](#)] [[PubMed](#)]
34. Kranz, M.; Sattler, B. Radiation dosimetry of the alpha(4)beta(2) nicotinic receptor ligand (+)-[(18)F]flubatine, comparing preclinical PET/MRI and PET/CT to first-in-human PET/CT results. *EJNMMI Phys.* **2016**, *3*, 25. [[CrossRef](#)] [[PubMed](#)]

35. Garrow, A.A.; Andrews, J.P.M. Preclinical dosimetry models and the prediction of clinical doses of novel positron emission tomography radiotracers. *Sci. Rep.* **2020**, *10*, 15985. [[CrossRef](#)]
36. Doss, M.; Kolb, H.C. Biodistribution and radiation dosimetry of the integrin marker 18F-RGD-K5 determined from whole-body PET/CT in monkeys and humans. *J. Nucl. Med.* **2012**, *53*, 787–795. [[CrossRef](#)] [[PubMed](#)]
37. Lobo, E.D.; Hansen, R.J. Antibody pharmacokinetics and pharmacodynamics. *J. Pharm. Sci.* **2004**, *93*, 2645–2668. [[CrossRef](#)]
38. Malik, P.; Phipps, C. Pharmacokinetic Considerations for Antibody-Drug Conjugates against Cancer. *Pharm. Res.* **2017**, *34*, 2579–2595. [[CrossRef](#)]
39. Sgouros, G. Bone marrow dosimetry for radioimmunotherapy: Theoretical considerations. *J. Nucl. Med.* **1993**, *34*, 689–694.
40. Macey, D.J.; Williams, L.E. *AAPM Report No 71, A Primer for Radioimmunotherapy and Radionuclide Therapy*; Medical Physics Publishing: Madison, WI, USA, 2001.
41. ICoR Protection. *Basic Anatomical and Physiological Data for Use in Radiological Protection: Reference Values*; ICRP Report No. 89; ICRP Publication: Pergamon, Turkey; Oxford, UK; New York, NY, USA, 2001.

Disclaimer/Publisher’s Note: The statements, opinions and data contained in all publications are solely those of the individual author(s) and contributor(s) and not of MDPI and/or the editor(s). MDPI and/or the editor(s) disclaim responsibility for any injury to people or property resulting from any ideas, methods, instructions or products referred to in the content.